Characterization of cellophane birefringence due to uniaxial strain by focused surface plasmon microscopy

Research Article Vol. 4, No. 2 / 15 February 2021 / OSA Continuum 409

Characterization of cellophane birefringence due to uniaxial strain by focused surface plasmon microscopy

IPSITA CHAKRABORTY AND HIROSHI KANO*

Muroran Institute of Technology, 27-1, Mizumoto-cho, Muroran, Hokkaido, 050-8585, Japan
h-kano@mmm.muroran-it.ac.jp

Abstract: In this paper, we study the relationship of local birefringence and stress oriented inhomogeneous elasticity of a sample from the spatial frequency response of focused surface plasmon (FSP). The birefringence of the sample varies the propagation constant of surface plasmon with regard to its direction and produces an elliptic absorption pattern in the reflected spatial frequency distribution. Birefringence is calculated from the ratio of the propagation constant along the fast to slow axis of the sample. The change in eccentricity was proportional to the applied stress on cellophane film. A strong correlation (0.94~0.97) exists between FSP and phase shifting interferometry results.

1. Introduction

Propagating surface plasmon (SP) at the flat interface of a conductor and a dielectric are essentially two-dimensional electromagnetic waves. Confinement on the metal surface is achieved since the propagation constant (β) is greater than the wave number (k) in the dielectric medium which leads to the evanescent decay in the dielectric medium [1]. Therefore, SPs cannot be excited directly by propagating light waves. The principal technique to satisfy the dispersion condition is achievable by use of a prism coupler as in Kretschmann's method [2]. In the case of Kretschmann's method, β is obtainable as the spatial frequency of the excitation light that gives the reflection minima. Since β shows strong dependency on the refractive index in the optical near-field from the metal surface, SPs can be a useful probe for determination of refractive index on the metal. Further, a microscope objective with high numerical aperture can be used instead of the prism coupler [3]. In this case, the SPs propagating in various directions on the metal surface can be excited and the interference of the SPs tend to localize/focus over a microscopic region corresponding to the optical diffraction limit with the introduction of focused laser beam as the source of excitation [4]. Thus, focused surface plasmon (FSP) allows label-free microscopic imaging based on index of refraction at the metal interface.

In refractive index measurements, dependency on direction of electric field oscillation of the probe beam appears for samples with anisotropy. Anisotropic samples, especially in thin film form are an integral part of optical technologies including polymers [5] and bio-medical cellular studies [6]. So, determination of the spatial distribution of anisotropy characteristics over the sample at specified sites of microscopic regions is a further requirement in bio-physical applications, where the existence of lateral heterogeneity (lipid domains [7], protein domains as amyloid [8], cell-electrode interaction in neuro-biology [9]) convey important (mechano-biological) functional information in real time. In other words, analysis of retardance essentially indicates quantitative measurement of the phase difference between the components of the amplitudes emerging from the specimen along its principal directions as well as identifying the direction of the fast axis with respect to a reference coordinate system [10]. The former is referred to as the magnitude of retardance and the latter as the direction of birefringence. Birefringence measurement have wide applicability in many fields involving polarized light such as electro-optic modulators [11],

#417743 https://doi.org/10.1364/OSAC.417743
Journal © 2021 Received 17 Dec 2020; revised 14 Jan 2021; accepted 14 Jan 2021; published 27 Jan 2021

OSA CONTINUUM

liquid crystal displays [12], laser resonator [13], non-linear optics [14] and bio-medical optics [15]. The principal technique for characterization of birefringence includes polarization rotation method with phase shifting interferometry [16] incorporating reconstruction algorithms [17] as potential examples. However, determination of spatially varying retardance calls for special techniques [18,19,20].

The use of SPs for characterizing anisotropy was also considered [21]. It was suggested that SPs excited by a similar optical setup for FSP, but with partial coherent light (in order to remove speckle noise, where the localization of SP is not achievable) could potentially provide the liquid-crystal birefringence by analyzing a reflected spatial frequency distribution.

We report for the first time that near field microscopic birefringence measurement can be realized with an optimized measurement probe. In this paper, we carry out local birefringent characterization of the anisotropic sample by launching FSP and collecting reflected light through a high numerical aperture microscope objective. In order to obtain birefringence of the sample, we analyzed the reflected spatial frequency distribution (i.e., the change in shape of the absorption pattern at the exit pupil). We used cellophane films as a sample and studied the spatial variance of birefringence due to inhomogeneous elasticity as a result of applied stress by FSP microscopy.

2. Theory

For the analysis, we consider the interface of a semi-infinite metal and anisotropic material as shown in Fig. 1(a). We consider the permittivity of the metal as ε_m and the anisotropic media has permittivity tensor in the form of ε. Also, the optic axis is parallel to the interface, i.e., lies on the x-y plane and α denotes the orientation of the optic axis with respect to the x- axis.

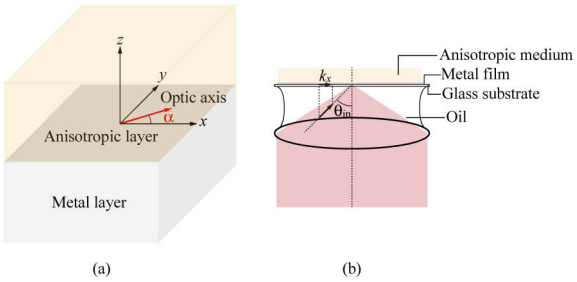

Fig. 1. (a) Metal-anisotropic interface with arbitrary orientation of birefringence, (b) FSP excitation with high NA objective lens.

Through, co-ordinate transformation the permittivity tensor for the anisotropic sample can be written as

$$\varepsilon = \begin{pmatrix} \varepsilon_a cos^2\alpha + \varepsilon_b sin^2\alpha & (\varepsilon_b - \varepsilon_a)\sin\alpha\ \cos\alpha & 0 \\ (\varepsilon_b - \varepsilon_a)\sin\alpha\ \cos\alpha & \varepsilon_a sin^2\alpha + \varepsilon_b cos^2\alpha & 0 \\ 0 & 0 & \varepsilon_c \end{pmatrix} \tag{1}$$

where ε_a, ε_b and ε_c are the dielectric constants along the principal directions, respectively.

Since surface plasmons are excited by p-polarized beam, we consider TM mode that propagates along the x-axis and its magnetic field along the y-axis of the structure. Applying boundary conditions for field components at the interface, the propagation constant can be derived as

$$k_{SP}^{aniso} = k_0 \sqrt{\frac{\varepsilon_m \varepsilon_c \left[\varepsilon_m - (\varepsilon_a cos^2\alpha + \varepsilon_b sin^2\alpha)\right]}{\varepsilon_m^2 - \varepsilon_c (\varepsilon_a cos^2\alpha + \varepsilon_b sin^2\alpha)}} \tag{2}$$

OSA CONTINUUM

where k_0 is the free space wave-number and ε_m is the dielectric constant of the metal, and for uniaxial anisotropic material, $n_0 = (\varepsilon_a)^2$ and $n_e = (\varepsilon_b)^2 = (\varepsilon_c)^2$. Fig. 1(b) depicts the surface plasmon excitation at the interface of metal and anisotropic media by using the FSP excitation scheme. The plane wave component involved in the converging light illuminate the interface of metal and anisotropic medium with a spatial frequency k_x that can be expressed by

$$k_x = k_0 n_{substrate} \sin\theta_{in} \tag{3}$$

where $n_{substrate}$ and θ_{in} denote the refractive index of glass substrate and incident angle, respectively. For coupling the photon to the SP, the dispersion matching condition is required, and it is expressed by

$$k_x = k_{SP}^{aniso} \tag{4}$$

The plane wave component satisfying the dispersion condition and having p-polarization can couple with SP which decays via heat dissipation during the propagation. Due to the energy consumption, an absorption minimum is observed in the reflected spatial frequency distribution that is observable at the exit pupil of the objective lens. The absorption pattern obtained at the exit pupil plane is elliptical due to the presence of anisotropic sample on the metal layer as described by Eq. (2).

3. Focused surface plasmon microscopy

The typical experimental set-up is shown in Fig. 2. The collimated He-Ne laser beam passed through a radial-polarization converter (RPC) which is placed in the conjugate plane of the entrance pupil of the oil-immersion microscope objective of N.A 1.65. The FSP was generated at the interface of the metal film and the anisotropic medium. The light reflected from the metal surface was collected by the same objective lens, and the Fourier transform of the same appeared at the exit pupil of the objective. The reflected spatial frequency distribution was acquired by an image sensor located in the conjugate plane of the pupil.

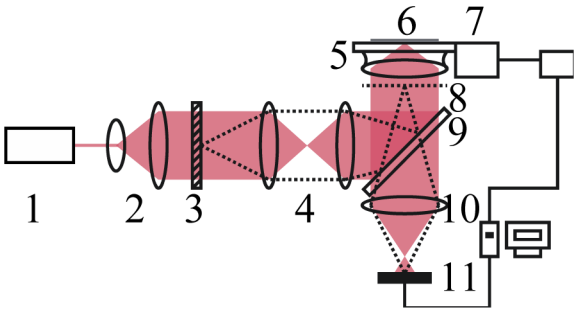

Fig. 2. Optical set-up with high NA objective lens. [1: He-Ne laser source (632.8 nm), 2: Beam Expander lenses, 3: Radial Polarization converter, 4: Telecentric lens system, 5: Oil immersion objective, 6: Sample, 7: Piezo-electric stage, 8: Exit Pupil, 9: Half mirror, 10: Focusing Lens, 11: CCD]

The substrate (cover slip with a refractive index of 1.78) was coated with a silver film with a thickness of 51nm and cellophane was used as anisotropic sample. As seen from Fig. 3(a), the sample when placed on the silver film do not produce any observable birefringence (absorption arcs are circular in nature) due to the presence of narrow air gap. We used a thin metal stripe to push the cellophane down to touch the silver thin film as shown in Fig. 3(b). The change in the nature of the absorption arcs (tending to be elliptical) indicate that the birefringence of the sample can be measured with this technique. The effect of uniaxial stretch on the sample is shown in Fig. 3(c), where the ellipticity of the absorption arcs changes further.

OSA CONTINUUM

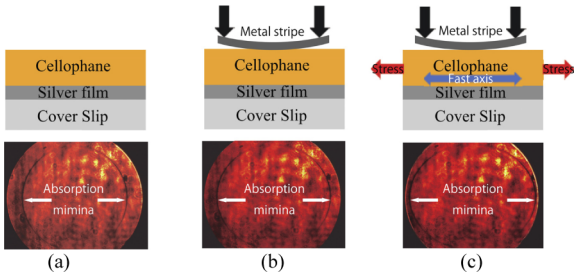

Fig. 3. Exit pupil image (a) with cellophane, (b) with introduction of metal stripe on cellophane, (c) with uniaxial stretch (blue arrow indicates fast axis of the sample while the red arrow shows the orientation of stretch).

4. Characterization of birefringence with influence of external factors

We determined the uniaxial strain dependence of refractive index anisotropy of cellophane with the help of phase shifting interferometry (PSI). For this purpose, we consider the sample to be placed in one arm of the Mach-Zehnder interferometer and four intensity frames (I_1, I_2, I_3 and I_4 respectively) are recorded with successive rotation of the polarizer in steps of 45° as shown in Fig. 4. The resultant retardance can be obtained as shown in Eq. (5).

$$\delta\,(x,y) = \frac{\lambda}{2\pi}\,\tan^{-1}\left(\frac{I_4(x,y) - I_2(x,y)}{I_3(x,y) - I_1(x,y)}\right) \tag{5}$$

Since the sample is stretched along its fast axis so the corrected birefringence can be obtained after the incorporation of the Poisson ratio with the simultaneous corrected thickness.

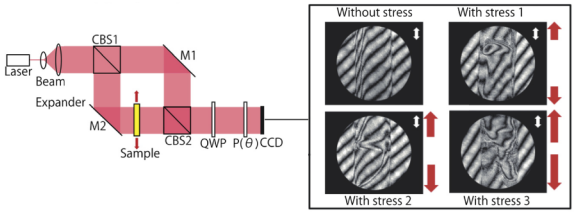

Fig. 4. Mach Zehnder interferometer with sample subjected to various degrees of stress as indicated by red arrows, (inset) Local retardance changes as observed at the CCD plane with the shift in fringes when various degrees of stress was applied to the sample (white arrow indicates orientation of fast axis of the sample).

To our knowledge, the results for Poisson ratio of cellophane were not available in literature and only known measurements were of cellulose I, cellulose II and cellulose Iβ [22]. We measured the Poisson ratio by direct mechanical stretching using a micrometer vise. The samples were cut from various sections of the same cellophane film and were stretched in a micrometer vise mounted on a micro positioning stage under a microscope. The stretching in the x-direction was varied from 0 to 25% determined by the micrometer reading. The change in width of the sample was measured using the micro positioning device with the help of the pre-positioned scale. A typical plot of the thickness versus the length of the sample is shown in Fig. 5. The slope of a straight-line fit (solid line in Fig. 5) to the data yields the Poisson ratio. Measurements were repeated on different samples obtained from various positions of the cellophane film. The average Poisson value was 0.43 and have been used throughout the analysis.

OSA CONTINUUM

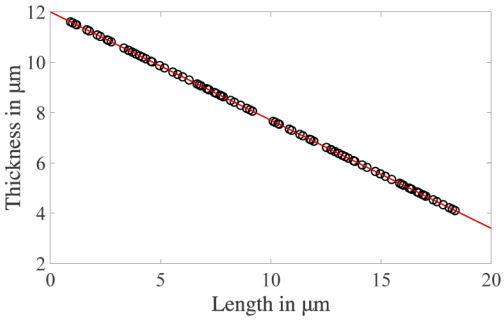

Fig. 5. Thickness vs length of the cellophane sample undergoing stretching of up to 25%. The black circles show the recorded data while the solid red line is the linear fit.

Thus, the birefringence of the sample is

$$\Delta n\ (x, y) = \frac{\lambda}{2\pi d_0 \left(1 - \sigma \frac{\Delta L}{L}\right)} \tan^{-1}\left(\frac{I_4(x,y) - I_2(x,y}{I_3(x,y) - I_1(x,y)}\right) \tag{6}$$

where, d_0 is the thickness of the sample before stretching, σ is the Poisson ratio obtained from the ratio of lateral strain to longitudinal strain, L is the length of the sample before stretching, ΔL is the effective change in length of the sample due to stretching.

Since all the parameters of Eq. (6) are determined we can reconstruct the spatial distribution of birefringence as shown in Fig. 6.

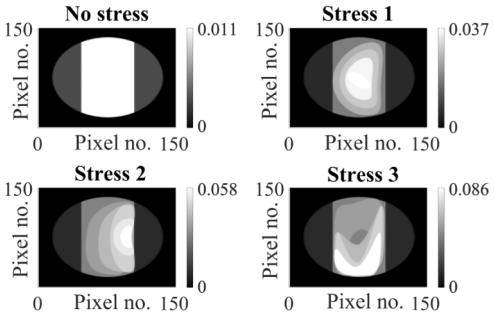

Fig. 6. Reconstructed birefringence map of sample when subjected to various degrees of stress.

Further, we calculate the k_{SP}^{aniso} with respect to the fast axis and slow axis of the sample and the ratio determines the eccentricity of the absorption ellipse at the exit pupil of the microscope for the four cases considering sample by changing the magnitude of applied stress (no stress, stress 1, 2, and 3). For this purpose, we best fit an ellipse to the data obtained from the absorption pattern and obtain the center co-ordinates of the ellipse and then determine the magnitude of the semi-major and the semi-minor axis pertaining to the oriented direction. The eccentricity is obtained by the ratio of the semi-major to the semi-minor axis of the ellipse and denotes the magnitude of birefringence. We obtain the values for four different positions of the samples as indicated by A, B, C, D due to the presence of spatial birefringence generated with stress as shown in Fig. 7 (blue data points). We also determined the birefringence of the samples maintained in previous conditions with phase shifting interferometry with the help of Eq.6 as discussed in the previous section for four positions of the sample as A', B', C' and D', respectively also shown in Fig. 7 (red data points). (The positions of the sample are closely related but are not exact as

OSA CONTINUUM

in A and A') We compare these results as obtained by FSP and PSI as shown in Fig. 7. One can see that there is a strong correlation of the birefringence and the position of the sample as obtained by PSI and FSP data. The Pearson's correlation co-efficient was obtained as 0.9497, 0.9569, 0.9684 and 0.9748 with root mean square error of 0.000837, 0.0030404, 0.002118 and 0.0036822 for no stress, stress 1, 2 and 3 respectively.

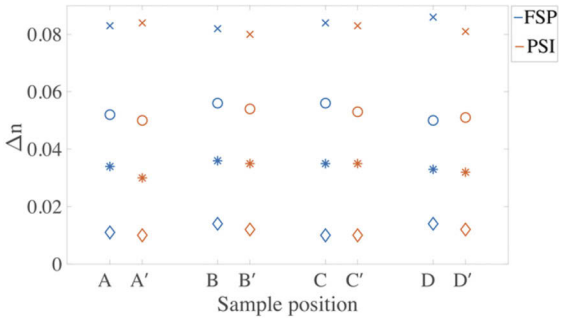

Fig. 7. Comparison of stress birefringence with focused surface plasmon (FSP) microscopy and phase shifting interferometry (PSI).[⋄:Without stretching, *: with stress 1, ∘: with stress 2 and ×: with stress 3]

Further to analyze the dependence of the optic axis orientation on the spatial frequency response of FSP from the exit pupil, we rotate the anisotropic sample in the plane perpendicular to the optical axis of the objective lens. We find that the rotation of the fast axis of the sample is manifested as a subsequent rotation of the elliptical absorption pattern in the exit pupil as shown in Fig. 8. We also analyzed the spatial frequency response of the sample when subjected to various environments such as temperature of 60°C and exposure to ultra-violet radiation (315–400 nm) for 24 hours as shown in Figs. 9(b) and 9(c), respectively. We find that the change in birefringence is manifested clearly from the change in eccentricity of the absorption ellipse as 1.8% and 10% respectively as shown in Figs. 9(b) and 9(c).

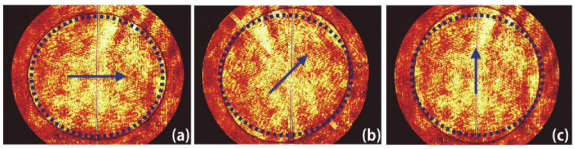

Fig. 8. Effect of rotation of the fast axis (indicated with blue arrow) of the sample on the exit pupil. Unstretched samples with fast axis orientation at (a) 0° (b) 45° and (c) 90°, respectively.

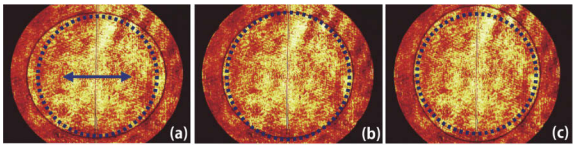

Fig. 9. Exit pupil when cellophane film was (b) stretched along its fast axis, (c) subjected to temperature of 60°C and (d) exposed to UV irradiation for 24 hours. The dotted pattern is for reference to the eye for the change in eccentricity.

OSA CONTINUUM

5. Conclusion

In this paper we studied the change in birefringence of the sample with uniaxial strain by spatial frequency response of focused surface plasmon microscopy. Later we correlated these measurements with phase shifting microscopy when the sample was maintained in previous conditions. It should be noted that this method can be applied to sub nano-meter thin film samples as well since confinement of FSP is within (~ 100 nm) from the metal film. This study can be particularly helpful for determining low birefringence changes due to certain mechano-biological activity in cellular environment in real time.

Acknowledgments. The first author would like to acknowledge the Ministry of Education, Culture, Sports, Science and Technology (MEXT), Japan for the scholarship.

Disclosures. The authors declare no conflicts of interest.

References

1. R. H. Ritchie, "Plasma Losses by Fast Electrons in Thin Films," Phys. Rev. **106**(5), 874–881 (1957).
2. E. Kretschmann and H. Raether, "Radiative decay of non-radiative surface plasmons excited by light," Z. Natur. Forsch **A23A**, 2135 (1968).
3. H. Kano, S. Mizuguchi, and S. Kawata, "Excitation of surface plasmon polaritons by a focused laser beam," J. Opt. Soc. Am. B **15**(4), 1381 (1998).
4. H. Kano, "Excitation of Surface Plasmon Polaritons by a Focused Laser Beam," in *Near-Field Optics and Surface Plasmon Polaritons. Topics in Applied Physics*, vol 81, Springer, Berlin, Heidelberg, (2001).
5. Ipsita Chakraborty and Hiroshi Kano, "Birefringence analysis of photo-addressable azopolymer thin films from spatial frequency response of focused surface plasmon," Proc. SPIE **11467**, 114671O (2020).
6. S. Woltman, G. Jay, and G. Crawford, "Liquid-crystal materials find a new order in biomedical applications," Nat. Mater. **6**(12), 929–938 (2007).
7. Z. Salamon, S. Devanathan, I. D. Alves, and G. Tollin, "Plasmon-waveguide resonance studies of lateral segregation of lipids and proteins into microdomains (Rafts) in solid-supported bilayers," J. Biol. Chem. **280**(12), 11175–11184 (2005).
8. E. Harté, N. Maalouli, A. Shalabney, E. Texier, K. Berthelot, S. Lecomte, and I. Alves, "Probing the kinetics of lipid membrane formation and the interaction of a nontoxic and a toxic amyloid with plasmon waveguide resonance," Chem. Commun. **50**(32), 4168–4171 (2014).
9. K. Toma, H. Kano, and A. Offenhäusser, "Label-Free Measurement of Cell–Electrode Cleft Gap Distance with High Spatial Resolution Surface Plasmon Microscopy," ACS Nano **8**(12), 12612–12619 (2014).
10. S. Sircar, I. Chakraborty, S. Roy, and K. Bhattacharya, "Full field retardation measurement of birefringent samples," Optik **150**, 22–28 (2017).
11. Y.-L. Lo and P.-F. Hsu, "Birefringence measurements by an electro-optic modulator using a new heterodyne scheme," *Opt. Eng.* 41(11) (2002).
12. G. Pathak, K. Agrahari, G. Yadav, A. Srivastava, O. Strzezysz, and R. Manohar, "Tuning of birefringence, response time, and dielectric anisotropy by the dispersion of fluorescent dye into the nematic liquid crystal," Appl. Phys. A **124**(7), 463 (2018).
13. Galina Machavariani, Yaakov Lumer, Inon Moshe, Avi Meir, Steven Jackel, and Nir Davidson, "Birefringence-induced bifocusing for selection of radially or azimuthally polarized laser modes," Appl. Opt. **46**(16), 3304 (2007).
14. Gunnar Arisholm, "General numerical methods for simulating second-order nonlinear interactions in birefringent media," J. Opt. Soc. Am. B **14**(10), 2543 (1997).
15. Chuanmao Fan and Gang Yao, "Mapping local optical axis in birefringent samples using polarization-sensitive optical coherence tomography," J. Biomed. Opt. **17**(11), 110501 (2012).
16. G. Lai and T. Yatagai, "Generalized phase-shifting interferometry," J. Opt. Soc. Am. A **8**(5), 822–827 (1991).
17. Daniel Malacara, *Optical Shop Testing* (Wiley, 2007), PP-568.
18. S. Sircar and I Chakraborty, "Birefringence Analysis Using Mach-Zehnder Interferometer", in Advances in Optical Science and Engineering. Springer Proceedings in Physics, vol 194. Springer, Singapore (2017).
19. S. Sircar and K. Bhattacharya, "Measurement of birefringence using polarization phase-shifting Mach–Zehnder interferometer," Opt. Eng. **54**(11), 113112 (2015).
20. P. Ghosh, S. S. Bhakat, I. Chakraborty, S. Sarkar, and K. Bhattacharya, "Extraction of phase profile at discrete spatial frequency bands using phase shifting interferometry," Proc. SPIE **11137**, 89 (2019).
21. T. Tanaka and S. Kawata, "Real-time observation of birefringence by laser-scanning surface plasmon resonance microscope," Opt. Express **13**(18), 6905 (2005).
22. K. Nakamura, M. Wada, S. Kuga, and T. Okano, "Poisson's ratio of cellulose Iβ and cellulose II," J. Polym. Sci., Part B: Polym. Phys. **42**(7), 1206–1211 (2004).